Synergistic Nanostructured MnO_x/TiO_2 Catalyst for Highly Selective Synthesis of Aromatic Imines

Putla Sudarsanam,*[a, b] Angela Köckritz,[a] Hanan Atia,[a] Mohamad Hassan Amin,[c] and Angelika Brückner*[a]

This work reports the development of a synergistic nanostructured MnO_x/TiO_2 catalyst, with highly dispersed MnO_x nanoparticles (4.5 ± 1 nm) on shape-controlled TiO_2 nanotubes (8–11 nm width and 120–280 nm length), for selective synthesis of valuable aromatic imines at industrially important conditions. Pristine TiO_2 nanotubes exhibited 97% imine selectivity at a 38.3% benzylamine conversion, whereas very low imine selectivity was obtained over commercial TiO_2 materials, indicating the catalytic significance of shape-controlled TiO_2 nanotubes. The MnO_x nanoparticle/TiO_2 nanotube (10 wt% Mn) catalyst calcined at 400 °C showed the best activity with 95.6% benzylamine conversion and 99.9% imine selectivity. This catalyst exhibited good recyclability for four times and is effective for converting numerous benzylamines into higher yields of imines. The high catalytic performance of MnO_x/TiO_2 nanotubes was attributed to higher number of redox sites (Mn^{3+}), high dispersion of Mn species, and shape-controlled structure of TiO_2, indicating that this catalyst could be a promising candidate for selective oxidation reactions.

Introduction

Selective catalytic oxidation processes provide a variety of valuable chemicals for the chemical industry.[1] Particularly, the selective oxidation of amines into imines is an important reaction because of many uses of the products for the synthesis of fine chemicals, pharmaceuticals, and biologically active compounds.[2] Liquid-phase catalysts with stoichiometric heavy metal oxidants and large quantities of organic solvents are often used for selective oxidation reactions to achieve satisfactory results. These catalytic protocols suffer from several drawbacks, such as high prices of catalysts/oxidants, their toxicity, huge amounts of waste generation, and inefficient catalyst recovery/reusability.[2d,3] Thus, developing eco-friendly and cost-effective catalytic routes is important for selective oxidation reactions, including amine oxidation into imines.

The combination of a heterogeneous solid catalyst with molecular oxygen under solvent-free conditions is certainly a promising strategy not only for amine oxidation, but also for other challenging oxidation reactions in organic synthesis. Molecular oxygen is the cheapest and the least polluting oxidizing agent. Nevertheless, pure O_2 in the presence of volatile organic chemicals/solvents at higher reaction temperatures/pressures bears safety risks as it may cause the explosion, which is a very serious problem for large scale synthesis of chemicals. Flammability risk can be prevented when oxidation reactions are performed by using diluted O_2 (e.g., 5 vol% O_2/Ar is used in this work).[4] An added benefit for amine oxidation is that imine product selectivity can be improved with small oxygen concentration in the reaction (Scheme 1). Several solid catalysts, especially supported noble metals (Au, Ru, Pd, Ag, etc.) have been found to be highly active for amine oxidation.[2a,3b,5] However, owing to the high price of noble metals and their limited availability, efforts have been made to develop alternative mono- and bi-metallic catalysts, mainly

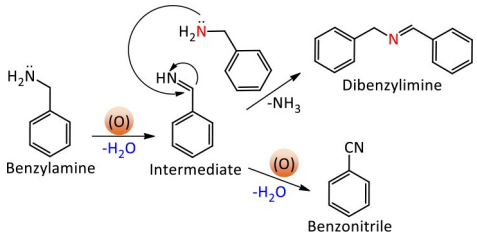

Scheme 1. Reaction pathways in the oxidation of benzylamine. Achieving higher amine conversion and product selectivity at industrially important conditions remains a great challenge.

[a] Dr. P. Sudarsanam, Dr. A. Köckritz, Dr. H. Atia, Prof. A. Brückner
Leibniz Institute for Catalysis e.V. (LIKAT)
Albert-Einstein-Str. 29a, 18059 Rostock (Germany)
E-mail: s.putla@ncl.res.in
Angelika.Brueckner@catalysis.de
[b] Dr. P. Sudarsanam
Catalysis and Inorganic Chemistry Division
CSIR-National Chemical Laboratory
Dr Homi Bhabha Road, Pashan, Pune 411008 (India)
[c] Dr. M. H. Amin
School of Science, RMIT University
Melbourne, Victoria 3001 (Australia)

Supporting information for this article is available on the WWW under https://doi.org/10.1002/cctc.202001870

This publication is part of a Special Collection on "Supported Nanoparticles and Single-Atoms for Catalysis: Energy and Environmental Applications". Please check the ChemCatChem "homepage for more articles in the collection".

based on Mn, Cu, Co, or Fe because of their tunable redox properties and abundant availability.[6]

Nanostructured TiO_2 is a promising material for a number of catalytic applications because of its unique structural, morphological, electrical, and redox properties. TiO_2 based nanomaterials have been widely used in photocatalytic applications including visible light-driven selective imines synthesis with excellent yields at mild reaction conditions.[7] However, their applications in thermochemical organic synthesis were rarely investigated. Under this scrutiny, we noticed an interesting work published by Klitgaard *et al.*, which highlighted the catalytic role of TiO_2 based materials for cyclohexylamine oxidation.[8] The structure-activity properties of nanostructured TiO_2 could be significantly modified by tuning its shape (nanotube, nanorod, nanoparticle, etc.).[9] The homogeneous dispersion of transition metal oxide nanoparticles (e.g., MnO_x) on shape-controlled TiO_2 may provide synergistic interface structures with enriched properties for selective catalysis. With this motivation, we developed a promising heterostructured catalyst, consisting of highly dispersed Mn-oxide nanoparticles on TiO_2 nanotubes, for solvent- and base-free oxidation of aromatic amines using 5 vol% O_2/Ar as the oxidant. Various analytical techniques, such as powder XRD, BET surface area, TEM, STEM-EDX, XPS, and H_2-TPR are used to understand structural, textural, redox, and morphology properties of MnO_x/TiO_2 nanocatalysts. This work not only reports a promising catalytic application of TiO_2 based nanomaterials for the synthesis of imine compounds at industrially important conditions, but also provides valuable insights for selective oxidation reactions.

Results and Discussion

Catalytic activity studies

Benzylamine oxidation as a model reaction was evaluated over a series of TiO_2 based catalysts and the results are shown in Table 1. This reaction typically follows two pathways, resulting in dibenzylimine and benzonitrile as major products as shown in Scheme 1.[2c] Initially, we performed a blank reaction (entry 1, Table 1), and only a 9.2% amine conversion was obtained. In the case of both TiO_2-NT400 and TiO_2-NT500 nanomaterials (entries 2 & 3, Table 1), amine conversion was increased to 34–38% with a high selectivity to imine (~97%), indicating the catalytic role of TiO_2 nanomaterials in benzylamine oxidation. In contrast, very low imine selectivity was found over commercial TiO_2 catalysts, with considerable amounts of oxime (entries 4 & 5, Table 1). It obviously indicates the promising role of nanostructured TiO_2 catalysts (Figure 3) to achieve improved imine selectivity in benzylamine oxidation.

Afterwards, we explored the catalytic activity of MnO_x (10 wt% metal) deposited on TiO_2-NT400, TiO_2-NT500, and commercial TiO_2 for benzylamine oxidation at similar reaction conditions used for pristine TiO_2 samples. Among the catalysts tested, the MnO_x/TiO_2-NT400 catalyst showed the best performance with a 95.6% benzylamine conversion (entry 6, Table 1).

Table 1. Aerobic oxidation of benzylamine over a series of nanostructured TiO_2 based catalysts.[a]

Entry	Catalyst	Amine conv. [%]	Selectivity [%]		
			Imine	Nitrile	Oxime
1	Blank	9.2	99.9	0.1	
2	TiO_2-NT400	38.3	97	0.1	2.8
3	TiO_2-NT500	34.6	97.6	0.1	2.3
4	TiO_2-Aldrich	36.5	73.8	0.9	25.3
5[b]	Aeroxide P25	18.4	20.8	5.2	11.9
6[c]	MnO_x/TiO_2-NT400	95.6	99.9	0.1	
7	MnO_x/TiO_2-Aldrich	57.8	98.7	1.3	
8	MnO_x/TiO_2-NT500	62.8	99.9	0.1	
9[d]	MnO_x/TiO_2-NT400	57.3	99.5	0.5	
10[e]	MnO_x/TiO_2-NT400	54.2	99.9	0.1	
11[f]	MnO_x/CeO_2	79.2	96.2	3.8	
12[g]	Mn_2O_3	81.7	94.3	5.7	

[a] Reaction conditions: 4 mmol benzylamine, 50 mg catalyst, 5 vol% O_2/Ar (oxidant), 5 bar initial pressure, 6 h reaction time, 120 °C reaction temperature, and no solvent/base. [b] Various non-identified products were seen in the GC. [c] 10 wt% Mn with respect to TiO_2. [d] 5 wt% Mn. [e] 25 mg catalyst. [f] 10 wt% Mn with respect to CeO_2 nanorods. [g] Catalyst amount: maintained the same mol% of Mn in Mn_2O_3 as in the 50 mg of MnO_x/TiO_2-NT400 catalyst.

Irrespective of the catalysts and the reaction conditions used, a high selectivity to imine product was obtained in this study. In the case of MnO_x/TiO_2-Aldrich catalyst calcined at 400 °C (entry 7, Table 1), only a 57.8% benzylamine conversion was obtained, which is very low compared to that of MnO_x/TiO_2-NT400 catalyst (entry 6, Table 1). It clearly indicates the favorable role of shape-controlled TiO_2 nanotubes in improving the catalytic activity of MnO_x/TiO_2 materials in benzylamine oxidation. This could be due to the synergistic catalytic effect of TiO_2 nanotube and MnO_x nanoparticle, which is discussed in the later section. Benzylamine conversion was decreased from 95.6% to 62.8% when the calcination temperature of MnO_x/TiO_2-NT catalyst increases from 400 to 500 °C (entry 8, Table 1). Similarly, low conversions of benzylamine were obtained for low Mn content (entry 9, Table 1) and low catalyst amount (entry 10, Table 1). It indicates the necessity of using a sufficient amount of Mn-oxide to obtain higher conversions in benzylamine oxidation. Low amine conversions were obtained over MnO_x/CeO_2 nanorods[3a] (entry 11, Table 1) and Mn_2O_3 (entry 12, Table 2), indicating the promising activity of MnO_x/TiO_2 nanotube catalyst in benzylamine oxidation at solvent-free conditions.

The effect of reaction temperature, reaction time, and reaction pressure on benzylamine oxidation was studied with the best MnO_x/TiO_2-NT400 catalyst. High imine selectivity (99.9%) was obtained at all reaction conditions (Figure 1 and Figure S1, Supporting Information). Amine conversion was increased from 28.7% at 90 °C to 39.4% at 100 °C (Figure 1a). Afterwards, amine conversion was significantly increased to 64.2 and 95.6% at 110 and 120 °C, respectively. Water, one of the by-products in benzylamine oxidation (Scheme 1), is considered to be a key factor for catalyst deactivation by blocking active sites. When the benzylamine oxidation is carried out at higher than 100 °C, the in-situ generated water would be mostly in vapor phase state in the autoclave reactor vessel. As a

Table 2. Selective oxidation of various aromatic amines using MnO_x/TiO_2-NT400 catalyst.[a]

Entry	Substrate	Amine conv. [%]	Imine sel. [%]	Nitrile sel. [%]
1	Benzylamine	95.6	99.9	0.1
2	*o*-Methoxybenzylamine	82.6	99.9	0.1
3	*m*-Methoxybenzylamine	99.2	99.9	0.1
4	*p*-Methoxybenzylamine	98.2	99.9	0.1
5	*p*-Methylbenzylamine	78.2	99.9	0.1
6	*p*-Chlorobenzylamine	89.6	99.9	0.1
7	*p*-Fluorobenzylamine	76.9	99.9	0.1
8	*o*-Bromobenzylamine	88.6	99.9	0.1
9[b]	Dibenzylamine	53.1	95.7	0.2
10	*n*-(tert-Butyl)benzylamine	7.3	99.9	0.1
11[c]	*n*-Butylamine	15.2	99.7	0.3

[a] 4 mmol benzylamine, 50 mg catalyst, 5 vol% O_2/Ar (oxidant), 5 bar initial pressure, 6 h reaction time, 120 °C reaction temperature, and no solvent. [b] Benzaldehyde (4.1%). [c] 65 °C reaction temperature.

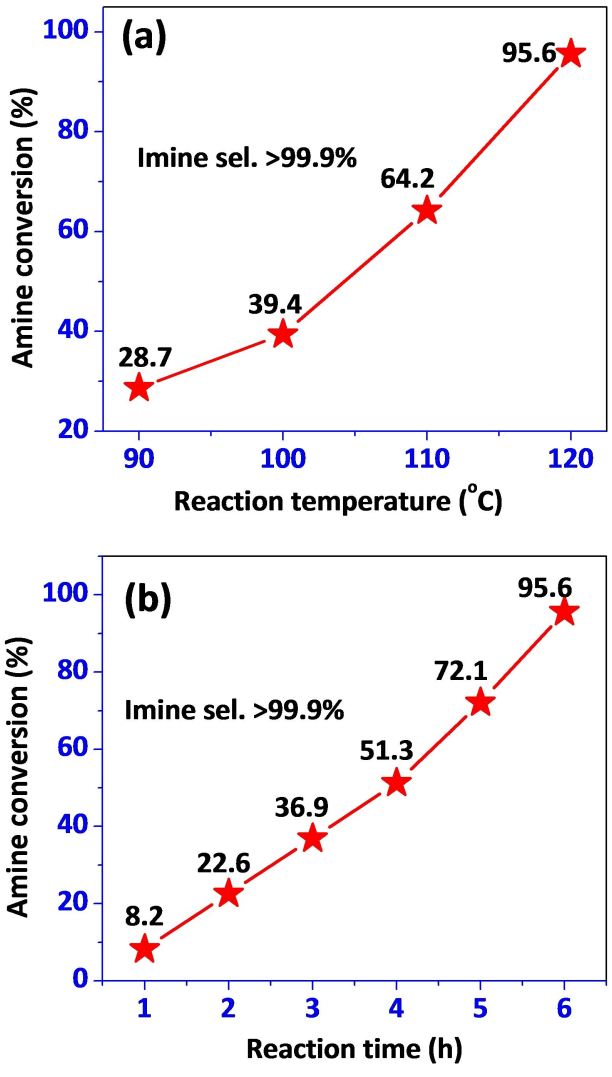

Figure 1. The behavior of benzylamine conversion with (a) reaction temperature and (b) reaction time over MnO_x/TiO_2-NT400 catalyst.

result, its accumulation on the catalyst surface will be negligible, which might be responsible for enhanced amine conversions at 110 and 120 °C. The kinetic profile of benzylamine oxidation shown in Figure 1b indicates that benzylamine was converted smoothly to the imine product during the first 4 h reaction while a further increase of benzylamine conversion was observed after 5 and 6 h. No intermediates were detected during the reaction. In addition, the performance of MnO_x/TiO_2-NT400 catalyst is dependent on the reaction pressure: about 48.9, 60.2, 72.6, 84.7 and 95.6% amine conversions were obtained at 1, 2, 3, 4, and 5 bar O_2, respectively (Figure S1, Supporting Information).

To evaluate the stability of the shape-controlled nanocatalysts, the recyclability of MnO_x/TiO_2-NT400 catalyst for benzylamine oxidation was studied up to four cycles and the results are shown in Figure 2. After completion of the reaction, the catalyst was recovered by centrifugation, washed with methanol three times, followed by oven drying at 100 °C for 2 h and subsequent heating to 400 °C for 4 h with 5 °C/min in static air. As shown in Figure 2, a continuous decrease in benzylamine conversion was found with repeated use of the catalyst, while maintaining high imine selectivity (99.7–99.9%). The weight loss of the catalyst (about 5%) during recovery/purification steps might be the reason for the decreased amine conversion during multiple uses of the catalyst. However, still more than 82% amine conversion with 99.9% imine selectivity was obtained after the fourth recycling test. It indicates that the nanostructured MnO_x/TiO_2 catalyst is stable and can be used as a promising recyclable heterogeneous catalyst for selective oxidations under mild reaction conditions.

Finally, the widespread applicability of MnO_x/TiO_2-NT400 catalyst was evaluated by testing its catalytic efficiency for the oxidation of various aromatic amines and the results are shown in Table 2. It was found that this catalyst efficiently converts the substituted benzylamines to the respective imine products under the conditions used for pure benzylamine. However, amine conversion strongly depends on the nature and position

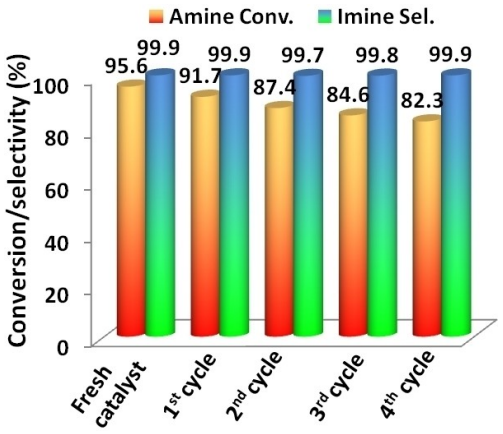

Figure 2. Recyclability of MnO_x/TiO_2-NT400 catalyst for benzylamine oxidation. Reaction conditions: 4 mmol benzylamine, 50 mg catalyst, 5 vol% O_2/Ar (oxidant), 5 bar initial pressure, 6 h reaction time, and 120 °C reaction temperature.

of the substituent. Lower amine conversions were obtained in the case of ortho-substituted methoxybenzylamine compared with meta- and para-substituted methoxybenzylamines (entries 2, 3 & 4, Table 2), which may be due to the steric hindrance effect of the ortho-substituent. Among different substituents in the para position, the highest conversion was obtained for *p*-methoxybenzylamine. This is probably due to the electron-donating effect of the methoxy group as it can enhance the coupling reaction between benzylamine and the intermediate to give the imine product (Scheme 1). Accordingly, higher conversion was obtained in the case of *p*-chlorobenzylamine (entry 6, Table 2) compared to *p*-fluorobenzylamine (entry 7, Table 2) as the fluoro group at the para position exhibits a strong electron-withdrawing effect. It indicates that, in addition to the steric influence of a substituent, its electronic properties play a crucial role in benzylamine oxidation. However, there was no much difference in amine conversion when chloro (entry 6, Table 2) and bromo groups (entry 8, Table 2) were present at the para and ortho positions, respectively. It should also be noted that substituents with different electronic effects at different positions can probably not be compared directly. On the other hand, low conversions were obtained in the case of bulky aromatic substrates (entries 9 and 10, Table 2). Surprisingly, a considerable amount of benzaldehyde was obtained in dibenzylamine oxidation reaction (entry 9, Table 2), which might stem from the hydrolysis of dibenzylimine into benzylamine and benzaldehyde.[10] The resulting benzylamine can undergo oxidative coupling (Scheme 1) to give the imine product, leaving the benzaldehyde behind. Improved conversions of substituted benzylamines were found when the reaction time was raised (Table S1, Supporting Information). Low conversion was found in the case of an aliphatic amine (entry 11, Table 2). It indicates that the presence of an active group (like benzyl) attached to the NH_2 of the amine seems to be essential to achieve higher conversions in amine oxidation.

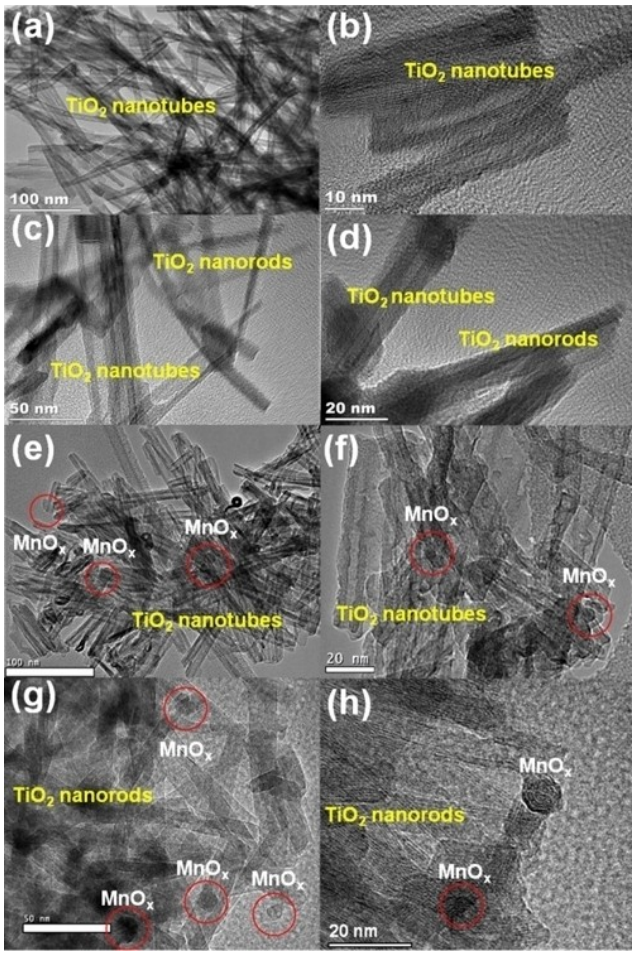

Figure 3. TEM images of TiO_2-NT400 (a,b), TiO_2-NT500 (c,d), MnO_x/TiO_2-NT400 (e,f), and MnO_x/TiO_2-NT500 (g,h) catalysts.

Characterization studies

Figure 3 shows TEM images of nanostructured TiO_2 and MnO_x/TiO_2 catalysts. Well-defined TiO_2 nanotubes with almost linear structures were formed (Figure 3a and 3b). The length of the TiO_2 nanotubes was found to be in the range of 120–280 nm and the width was about 8–11 nm. Upon increase of the calcination temperature from 400 to 500 °C, changes in TiO_2 morphology were noticed, exhibiting both nanotube and nanorod structures (Figure 3c and 3d). Furthermore, the average inner diameter (3.4 nm) of TiO_2 nanotubes in the material calcined at 500 °C (TiO_2-NT500) is lower compared to that calcined at 400 °C (4.5 nm). This indicates partial coalescence of cavities in TiO_2 nanotubes with rising temperature, which reduces the inner diameter and could also be a reason for the formation of nanorod structures in TiO_2-NT500. In the case of MnO_x/TiO_2-NT400 catalyst (Figure 3e and 3f), the morphology of TiO_2 nanotubes remains unchanged. Unlike in pure TiO_2-NT500 that shows both nanotube and nanorod structures (Figure 3c and 3d), only nanorod structures were found in MnO_x/TiO_2-NT500 catalyst (Figure 3g and 3h). This is probably due to the combined effect of higher calcination temperatures and impregnated MnO_x species in tuning TiO_2 morphology from nanotubes to nanorods. Regardless of calcination temperature used, nearly spherically shaped MnO_x nanoparticles were formed in MnO_x/TiO_2 catalysts, being larger in MnO_x/TiO_2-NT500 (7.5 ± 1 nm) compared to MnO_x/TiO_2-NT400 (4.5 ± 1 nm). This suggests that higher calcination temperature promotes the agglomeration of MnO_x. The TEM image (Figure S2, supporting information) of the used MnO_x/TiO_2-NT400 catalyst reveals an increase in the size of the MnO_x particles (8.5 ± 1 nm). However, the shape of the TiO_2 nanotubes is not changed after the reaction. Hence, an increase in the particle size of MnO_x, along with the catalyst's weight loss could be the reason for the decreased amine conversion with the repeated use of the catalyst (Figure 2).

To determine metal dispersion in MnO_x/TiO_2 nanomaterials, the STEM-EDS elemental mapping analysis was performed (Figure 4). Clearly, highly dispersed Mn species were formed in MnO_x/TiO_2-NT400 material, whereas aggregated Mn clusters were found in MnO_x/TiO_2-NT500 material, in line with the particle sizes obtained from TEM studies (Figure 3e–h). The

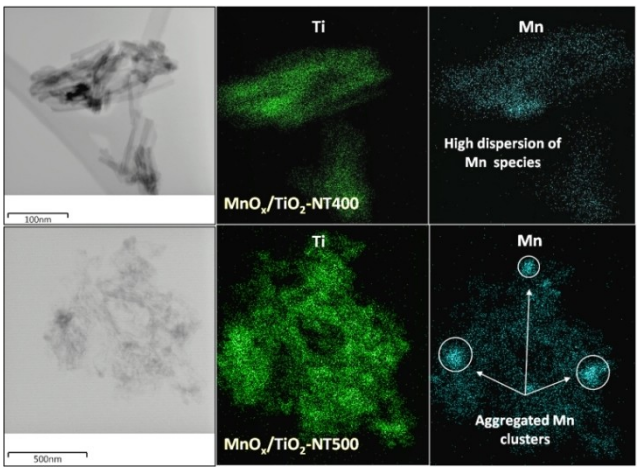

Figure 4. STEM-EDS elemental mapping images of MnO_x/TiO_2-NT400 and MnO_x/TiO_2-NT500 catalysts.

difference in particle size of MnO_x and TiO_2 morphology can considerably affect the MnO_x–TiO_2 interactions with an important role on the catalytic performance of nanostructured MnO_x/TiO_2 catalyst. Powder XRD profiles of nanostructured TiO_2 and MnO_x/TiO_2 catalysts are shown in Figure S3 (Supporting Information). Pristine TiO_2 materials mainly exhibit reflections of an anatase phase at two theta values of 25.3, 37.8, 48.1, 53.9, 55.1, 63.7, 68.9, 70.8, 75.9 and 82.9°.[9a] Interestingly, there was no obvious variation in the XRD peaks' position and intensity when the calcination temperature of TiO_2 was raised from 400 to 500 °C. This confirms that, despite the morphology changes as observed by TEM analysis (Figure 3a–d), the TiO_2 nanomaterial shows excellent phase stability in the applied range of calcination temperature. In contrast, the addition of MnO_x led to a drastic change in the peaks' intensity/width of TiO_2, indicating modifications in the crystal structure and crystallite size of TiO_2. As evident from Figure S3 (Supporting Information), reflections of rutile TiO_2 were found in MnO_x/TiO_2-NT500 at two theta values of 27.49, 36.1, 41.3, and 56.6°.[11] No characteristic peaks corresponding to MnO_x were found.[12] There could be two possible reasons for this observation, namely amorphous nature of the MnO_x particles and/or their high dispersion on TiO_2.

All materials exhibit type IV isotherm with H3-type hysteresis loop (Figure S4, Supporting Information), which indicates the presence of slit-shaped pores. As shown in Table 3, TiO_2-NT400 exhibits a higher BET surface area (203 m^2/g), which is however considerably decreased to 180 m^2/g after MnO_x addition. This is due to the penetration of MnO_x species into the pores and/or cavities of TiO_2 nanotubes. A drastic decrease in the BET surface area (123 m^2/g) of TiO_2 nanotubes is noticed when the calcination temperature increases from 400 to 500 °C (TiO_2-NT500). This is probably due to the changes in TiO_2 morphology (Figure 3a–d). TiO_2 nanotubes are formed via the folding of titanate nanosheets and folding usually leads to the higher surface area. Cavities present in TiO_2 nanotubes could also be the reason for its high BET surface area. On the other hand, partial collapse of hollow TiO_2 nanotubes to nanorods was observed at 500 °C (Figure 3c,d). This might reduce the inner surface area. However, there was no much variation in the BET surface area of TiO_2-NT500 material after MnO_x impregnation (MnO_x/TiO_2-NT500: 120 m^2/g). As well, the effect of Mn loading on the BET surface area of MnO_x/TiO_2-NT400 catalyst is negligible: 180 and 186 m^2/g values were obtained for 10 and 5 wt% Mn loaded catalysts. The average pore diameter of TiO_2 and MnO_x/TiO_2 materials was found to be in the range of 10–20 nm. A linear correlation between pore volume and BET surface area for the materials was found: the higher the pore volume of the catalyst, the higher is the BET surface area. Hence, TiO_2-NT400 material shows higher values of both BET surface area and pore volume (Table 3).

Table 3. BET surface area (BET SA), pore diameter, and pore volume of TiO_2 and MnO_x/TiO_2 catalysts.

Catalyst	BET SA [m^2/g]	Pore diameter [nm]	Pore volume [cm^3/g]
TiO_2-NT400	203	12.398	0.728
10 MnO_x/TiO_2-NT400	180	12.625	0.664
TiO_2-NT500	123	20.008	0.649
10 MnO_x/TiO_2-NT500	120	17.709	0.635
5 MnO_x/TiO_2-NT400	186	10.712	0.712

H_2-TPR analysis was performed to study the catalysts' reducibility and oxidation states of Mn in MnO_x/TiO_2 catalysts (Figure 5), and this information is important to understand the role of these factors in benzylamine oxidation reaction. For each catalyst, two reduction peaks were found in the range of 200–750 °C. TiO_2 is not reduced below 500 °C.[13] Hence, the peaks observed below 500 °C in TPR profiles belong to MnO_x species. The position of TPR peaks and their intensity in MnO_x/TiO_2-Aldrich catalyst are quite different compared to those of the nanostructured MnO_x/TiO_2 catalysts. This suggests the presence of various Mn-oxide species, which may differ in their oxidation state and interaction strength with TiO_2 support.[12,14] The MnO_x/TiO_2-Aldrich catalyst shows two reduction peaks centered at 315 °C and 407 °C, which correspond to the reduction of MnO_2 to Mn_2O_3 and Mn_2O_3 to Mn_3O_4, respectively. It is interesting to note that the peak corresponding to the reduction of MnO_2 to Mn_2O_3 is not observed in nanostructured MnO_x/TiO_2 catalysts, indicating the absence of Mn^{4+} species. However, the peak corresponding to the reduction of Mn_2O_3 to

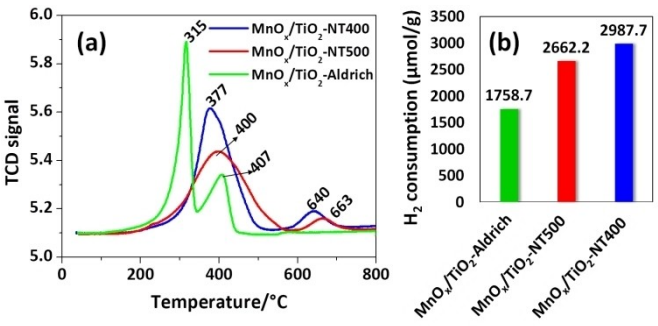

Figure 5. (a) H_2-TPR profiles and (b) H_2 consumption of MnO_x/TiO_2 catalysts.

Mn_3O_4 is shifted to lower temperatures i.e. 377 and 400 °C for MnO_x/TiO_2-NT400 and MnO_x/TiO_2-NT500, respectively, compared to the MnO_x/TiO_2-Aldrich catalyst (407 °C). Furthermore, the intensity of this peak is the highest for nanostructured MnO_x/TiO_2 catalysts, indicating the presence of more number of Mn^{3+} species in these samples compared to that of MnO_x/TiO_2-Aldrich catalyst. As reported by Chen *et al.*,[15] manganese oxide had a superior catalytic activity and imine selectivity in benzylamine oxidation, due to the abundant active sites (Mn^{3+}), which possess excellent redox properties. In addition, a broad reduction peak is observed at higher temperatures (after 640 °C) for nanostructured MnO_x/TiO_2 catalysts. This peak can be ascribed to the reduction of Ti species in TiO_2 or Mn–Ti–O solid solution.[16] Surprisingly, this peak is not observed in MnO_x/TiO_2-Aldrich catalyst. This may suggest that a tight connection between MnO_x and TiO_2 leads to the formation of Mn–O–Ti moieties at their interface in the nanostructured MnO_x/TiO_2 catalysts. Consumption of hydrogen during TPR studies was found to be higher for nanostructured MnO_x/TiO_2 catalysts, compared to conventional MnO_x/TiO_2-Aldrich catalyst (Figure 5b). This suggests the presence of more redox sites (Mn^{3+}) in nanostructured MnO_x/TiO_2 catalysts. The amount of H_2 reduced could be related to some Ti^{4+} species that are in interaction with Mn^{3+} because the amount of theoretical H_2 needed to reduce Mn^{4+} to Mn^{2+} is about 1820 μmol/g, which is low compared to that of nanostructured MnO_x/TiO_2 catalysts. Overall, the MnO_x/TiO_2-NT400 catalyst exhibits higher number of Mn^{3+} species (a high-intensity peak at 307 °C, corresponding to Mn_2O_3 to Mn_3O_4) and a higher number of redox sites.

XPS analysis was done to further understand the redox nature of MnO_x species in MnO_x/TiO_2 catalysts. As shown in Figure 6, two peaks were observed in MnO_x/TiO_2-NT400 and MnO_x/TiO_2-NT500 catalysts. In contrast, the MnO_x/TiO_2-Aldrich catalyst exhibits three peaks. The peaks observed at 640.4–640.7 and 641.9–642.5 eV correspond to Mn^{2+} and Mn^{3+}, respectively, while the peak noticed at 644.2 eV corresponds to Mn^{4+}.[12] Thus, the nanostructured MnO_x/TiO_2 catalysts contain only Mn^{2+} and Mn^{3+}, while the MnO_x/TiO_2-Aldrich catalyst contains three oxidation states of Mn (Mn^{2+}, $Mn^{3+}$and Mn^{4+}), in line with the H_2-TPR studies (Figure 5).

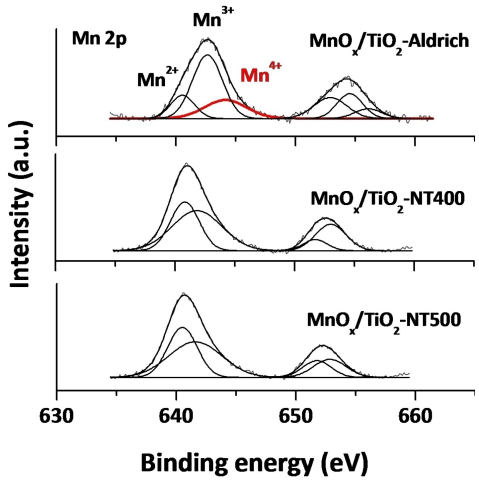

Figure 6. Mn 2p XP spectra of MnO_x/TiO_2 catalysts.

Key factors for the observed catalytic results

The catalytic activity results revealed that pure TiO_2 exhibits about 18–38% benzylamine conversion (entries 2–5, Table 1), while only about 9% amine conversion was achieved under blank conditions (entry 1, Table 1). This reveals that TiO_2 is certainly a catalytically active material for benzylamine conversion, while giving high imine selectivity, especially in the case of nanostructured TiO_2 materials (entries 2 & 3, Table 1). Both acid and redox sites are needed for benzylamine oxidation to obtain imine product. For instance, the acidic properties of metal oxides like CeO_2 play a key role in benzylamine oxidation to imine product.[17] It is a well-known fact that TiO_2 exhibits abundant Lewis acid sites, due to the presence of coordinatively unsaturated Ti^{4+} species, which might contribute to its catalytic activity in this reaction.[18] With commercial TiO_2 materials, a higher selectivity to oxime is achieved (entries 4 & 5, Table 1) besides imine. Klitgaard *et al.*, reported that oxime is formed via oxidation of amine with molecular oxygen over TiO_2 based catalysts.[8] Surprisingly, the shape-controlled TiO_2 nanomaterials (entries 2 & 3, Table 1) show much higher imine selectivities and negligible oxime formation, indicating their promising role in achieving high product selectivity in aerobic benzylamine oxidation. A significant finding of this work is that the addition of MnO_x to TiO_2 nanotubes led to an enhanced benzylamine conversion (95.6%, entry 6, Table 1), which is higher compared to that of TiO_2 nanotubes (entry 2, Table 1) and Mn_2O_3 (entry 12, Table 1). This indicates a synergistic catalytic effect between MnO_x nanoparticle and TiO_2 nanotube for benzylamine oxidation. The oxime product was not formed in the case of MnO_x/TiO_2-Aldrich catalyst. This suggests that MnO_x species are favorable towards imine product.

Some controlled experiments were conducted to understand the role of BET surface area of the catalysts in benzylamine oxidation. There is no much difference in amine conversion over TiO_2-NT400 (entry 2, Table 1) and TiO_2-NT500 (entry 3, Table 1) catalysts, whose BET surface areas are 203 and 123 m^2/g (Table 3), respectively. Both 10 wt% MnO_x/TiO_2-NT400 and 5 wt% MnO_x/TiO_2-NT400 catalysts show almost same BET surface area (Table 3). However, 10 wt% MnO_x/TiO_2-NT400 catalyst exhibited a 95.6% amine conversion (entry 6, Table 1), while only 57.3% amine conversion was achieved over 5 wt% MnO_x/TiO_2-NT400 catalyst (entry 9, Table 1). Therefore, the BET surface area of the catalysts is not a key factor for the catalytic activity of TiO_2 and MnO_x/TiO_2 catalysts for benzylamine oxidation. It was found that MnO_x/TiO_2-NT400 catalyst exhibits a higher number of redox sites (Figure 5). Smaller sized MnO_x nanoparticles (Figure 3e–f) and uniform dispersion of Mn species on TiO_2 nanotubes (Figure 4) are further unique characteristics of MnO_x/TiO_2-NT400 catalyst. Controlling particle size, as noticed in MnO_x/TiO_2-NT400 catalyst, can provide the uniform geometry of catalytic active sites, which could be a reason for achieving higher amine conversions over this

catalyst. It is also possible that O species from the small MnO_x particles do the oxidation according to a Mars-van Krevelen mechanism ($Mn_2O_3 \rightarrow Mn_3O_4$). Due to the smaller particles, a higher number of such O species is available in the 400 °C calcined sample i.e. MnO_x/TiO_2-NT400 compared to the 500 °C sample. Therefore, the high catalytic performance of MnO_x/TiO_2 nanotubes was attributed to higher amounts of redox sites, uniform dispersion of Mn species, and shape-controlled structure of TiO_2 nanotubes. A careful observation of the reaction conditions reported in Table 4 for benzylamine oxidation over various heterogeneous catalysts indicates that the nanostructured MnO_x/TiO_2 catalyst exhibits good amine conversion and high imine selectivity at industrially relevant mild conditions without using any organic solvent.

Conclusions

A highly selective catalytic route for aromatic imines via aerobic oxidative coupling of benzylamines using a heteronanostructured MnO_x/TiO_2 catalyst was reported in this work. A synergistic effect between shape-controlled TiO_2 nanotubes and MnO_x nanoparticles was demonstrated for imines synthesis at mild reaction conditions without using a solvent and base. A 95.6% benzylamine conversion with 99.9% imine selectivity was achieved over the MnO_x/TiO_2 nanotube-based catalyst (10 wt% Mn) calcined at 400 °C. This catalyst was also found to be effective for the aerobic oxidative coupling of various benzylamines at mild reaction conditions, exhibiting an excellent selectivity to imine products (>99%) at moderate to good conversion rates. A minor loss in benzylamine conversion was found after the 4th recycling test of MnO_x/TiO_2 nanotubes, while maintaining high imine selectivity. Higher amounts of redox sites (especially Mn^{3+}), high dispersion of Mn species, and shape-controlled structure of TiO_2 nanotubes are found to be key factors for high catalytic performance of MnO_x/TiO_2 nanotubes in benzylamine oxidation.

Experimental Section

Catalysts synthesis

An alkaline-assisted hydrothermal method was used for synthesizing shape-controlled TiO_2 nanotubes, which involves the dispersion of TiO_2 powder (Sigma Aldrich) in 5 mL of deionized water under ultrasonication treatment for 5 min.[9a] Then, 10 M NaOH (70 mL) was added drop-wise to the TiO_2 suspension under mild stirring conditions at room temperature and the stirring was continued for another 30 min to obtain a homogeneous suspension. The sample was taken into a 100 mL Teflon-lined autoclave and the hydrothermal treatment was carried out in an oven at 140 °C for 20 h. After cooling the autoclave to room temperature, the sample was collected by centrifugation and washed with deionized water and 0.1 M HNO_3 several times until the pH of the solution reaches 7. Finally, the material was dried at 95 °C for 10 h in an oven and subsequently calcined at 400 and 500 °C for 4 h under static air conditions. The samples were denoted as TiO_2-NT400 and TiO_2-NT500 (NT – nanotube; 400 and 500 are the calcination temperatures).

The MnO_x/TiO_2-NT catalysts (10 wt% of Mn with respect to TiO_2) were prepared using a wet-impregnation method.[19] Initially, the Mn precursor was taken into the deionized water under mild stirring conditions, followed by the addition of as-synthesized TiO_2 at room temperature. The temperature of the suspension was initially increased to 65 °C, maintained for 1 h under stirring to enhance the adsorption of Mn species on TiO_2 surface. Then, the temperature was increased to 95 °C and maintained until all the water is evaporated under stirring. The MnO_x/TiO_2-NT sample was dried at 95 °C for 10 h and then, calcined at 400 and 500 °C for 4 h under static air conditions. For comparison, a conventional MnO_x/TiO_2 catalyst using TiO_2 (Aldrich) was also prepared using the same conditions.

Characterization studies

A Bruker D4 Endeavor instrument equipped with a PSD LynxEye detector and a Cu Kα radiation source was used to obtain the powder XRD data (two theta range of 10–85°, a step size of 0.03° and a step time of 2.5 s) of the nanostructured catalysts. The TEM-HRTEM images were obtained using a JEOL 2100F with a Gatan Orius SC1000 CCD camera. The elemental mapping images of MnO_x/TiO_2 catalysts were obtained using an EDS spectrometer (Oxford XMax80T) in STEM mode. An ESCALAB 220 iXL X-ray photoelectron spectrometer (ThermoFisher) was used to estimate metal oxidation states and surface composition in nanostructured

Table 4. Comparison of the activity of nanostructured MnO_x/TiO_2-NT400 catalyst with the reported heterogeneous catalysts.

Catalyst	Benzylamine conv. [%]	Imine sel. [%]	Reaction conditions	Ref.
Ce–Sm/SiO_2	69	99.9	2 mmol amine, 200 mg catalyst, 20 mL min^{-1} O_2 bubbling rate, 4 h, 120 °C, no solvent	[17]
MoS_2/rGO[a]	91	97	0.5 mmol amine, 5 mg catalyst, 2.5 mL *n*-octane, 120 °C, O_2 (1 atm), 20 h	[20]
PdCu	94	92.1	200 μL amine, 20 mg catalyst, 110 °C, 3 h, atm O_2, no solvent	[21]
Au/CF[b]	99	99.9	2 mmol amine, 200 mg catalyst, 20 mL min^{-1} O_2 bubbling rate, 7 h, 130 °C, no solvent	[22]
Cu-doped CeO_2	97.8	98.6	3 mmol amine, 3 mL dimethyl sulfoxide, 0.3 mmol *n*-hydroxyphthalimide, 50 mg catalyst, 48 h, 110 °C, air	[6b]
UiO-66(Ce) MOF[c]	97	95	0.5 mL amine, 50 mg catalyst, O_2 purging, 12 h, 120 °C	[23]
Manganese oxide	100	96.2	1 mmol amine, 25 mg catalyst, 110 °C, 2 h, air balloon, 5 mL toluene	[15]
MnO_x/TiO_2	95.6	99.9	4 mmol amine, 50 mg catalyst, 120 °C, 6 h, 5 vol% O_2/Ar, 5 bar pressure, no solvent	Present work

[a] rGO: Reduced graphene oxide. [b] CF: CeO_2–Fe_2O_3. [c] MOF: Metal-organic framework.

MnO_x/TiO_2 catalysts at room temperature using monochromatic AlK_α radiation. With reference to the C 1s value of 284.8 eV, the binding energies of all metals in the nanostructured catalysts were charge corrected. The specific surface area, pore size, and pore volume of the catalysts were estimated using nitrogen adsorption-desorption analysis at −196 °C (liquid N_2 temperature). For this, an ASAP 2010 M characterization unit (Micromeritics) was used. Prior to analysis, samples were degassed at 400 °C for 2 h under vacuum. The specific surface area and pore size distribution were determined using the BET equation and the BJH model, respectively. A Micromeritics Autochem II 2920 instrument was used for the H_2-TPR studies of the catalysts. About 60 mg sample was loaded in a U-shaped quartz reactor and heated from room temperature to 400 °C with 10 °C/min in 5% O_2/He (50 ml/min) for 30 min. The sample was cooled down to room temperature under the flow of 5% O_2/He and then was flushed with Ar for 30 min. The TPR measurement was carried out from room temperature to 900 °C (holding time is 30 min) in a 5% H_2/Ar flow (50 ml/min) with a heating rate of 10 °C/min. A thermal conductivity detector was used to record the hydrogen consumption peaks with temperature and based on the peak areas, the quantitative analysis of the hydrogen consumption was estimated.

Catalytic activity studies

The benzylamine oxidation reaction was carried out at industrially important conditions in an autoclave reactor using 5 vol% O_2/Ar (oxidant), 5 bar initial pressure, 6 h reaction time, and 120 °C reaction temperature under solvent- and base-free conditions. For each reaction, 4 mmol benzylamine and 50 mg catalyst were taken in a glass vial, which was placed inside an autoclave reactor and the reaction was carried out at the appropriate conditions. The effect of various reaction conditions, such as temperature, pressure, and time was investigated using MnO_x/TiO_2-NT400 catalyst (10 wt% Mn). After the reaction, the liquid sample was separated from the solid catalyst by centrifugation. The amine conversion and product selectivity were determined by gas chromatography (SHIMADZU GC/MS-QP 2010S device) equipped with a flame ionization detector and an Optima 5MS column (50 m × 0.32 mm × 0.50 μm, split 1:50, external standard diethylene glycol dibutyl ether).

Acknowledgements

PS would like to thank DAAD (Germany) for Leibniz-DAAD postdoctoral fellowship-2016 (personal ref. no.: 91632777). The authors acknowledge the support from RMIT Microscopy and Microanalysis Facility Centre for TEM and STEM-EDX studies. Open access funding enabled and organized by Projekt DEAL.

Conflict of Interest

The authors declare no conflict of interest.

Keywords: Nanostructured catalyst · Selective catalysis · Aerobic oxidation · Acid-redox properties · Synergistic metal-oxide interaction

[1] Z. Guo, B. Liu, Q. Zhang, W. Deng, Y. Wang, Y. Yang, *Chem.Soc. Rev.* **2014**, *43*, 3480–3524.
[2] a) R. Ray, S. Chandra, V. Yadav, P. Mondal, D. Maiti, G. K. Lahiri, *Chem. Commun.* **2017**, *53*, 4006–4009; b) A. Han, H. Zhang, G.-K. Chuah, S. Jaenicke, *Appl. Catal. B: Environ.* **2017**, *219*, 269–275; c) M. T. Schümperli, C. Hammond, I. Hermans, *ACS Catal.* **2012**, *2*, 1108–1117; d) B. Chen, L. Wang, S. Gao, *ACS Catal.* **2015**, *5*, 5851–5876.
[3] a) P. Sudarsanam, B. Hillary, M. H. Amin, S. B. A. Hamid, S. K. Bhargava, *Appl. Catal. B: Environ.* **2016**, *185*, 213–224; b) P. Sudarsanam, B. Mallesham, A. Rangaswamy, B. G. Rao, S. K. Bhargava, B. M. Reddy, *J. Mol. Catal. A* **2016**, *412*, 47–55.
[4] C. Parmeggiani, C. Matassini, F. Cardona, *Green Chem.* **2017**, *19*, 2030–2050.
[5] a) S. Furukawa, A. Suga, T. Komatsu, *Chem. Commun.* **2014**, *50*, 3277–3280; b) S. Wu, W. Sun, J. Chen, J. Zhao, Q. Cao, W. Fang, Q. Zhao, *J. Catal.* **2019**, *377*, 110–121; c) J. Meilin, A. Wulan, B. Yongsheng, C. Xiaowei, Sagala, W. Jiang, Zhaorigetu, *Rare Met. Mat. Eng.* **2018**, *47*, 442–446; d) J. Mielby, R. Poreddy, C. Engelbrekt, S. Kegnæs, *Chin. J. Catal.* **2014**, *35*, 670–676.
[6] a) J. Bu, W. Wang, H. Zhang, C. Wu, B. Zhang, Y. Cao, F. Zhou, Q. Zhang, X. Zhang, *Mol. Catal.* **2018**, *459*, 46–54; b) X. Huang, G. Lu, K. Zhang, J. Liu, H. Zhang, Z. Guo, J. Tao, *Appl. Surf. Sci.* **2020**, *514*, 145948; c) C. Zhang, P. Zhao, Z. Zhang, J. Zhang, P. Yang, P. Gao, J. Gao, D. Liu, *RSC Adv.* **2017**, *7*, 47366–47372; d) L. Geng, W. Jian, P. Jing, W. Zhang, W. Yan, F.-Q. Bai, G. Liu, *J. Catal.* **2019**, *377*, 145–152; e) M. N. Pahalagedara, L. R. Pahalagedara, D. Kriz, S.-Y. Chen, F. Beaulieu, W. Thalgaspitiya, S. L. Suib, *Appl.Catal. B: Environ.* **2016**, *188*, 227–234.
[7] a) H. Xu, J.-L. Shi, H. Hao, X. Li, X. Lang, *Catal.Today* **2019**, *335*, 128–135; b) X. Li, H. Xu, J.-L. Shi, H. Hao, H. Yuan, X. Lang, *Appl. Catal. B: Environ.* **2019**, *244*, 758–766; c) X. Lang, H. Ji, C. Chen, W. Ma, J. Zhao, *Angew. Chem. Int. Ed.* **2011**, *50*, 3934–3937; *Angew. Chem.* **2011**, *123*, 4020–4023; d) X. Lang, W. Ma, Y. Zhao, C. Chen, H. Ji, J. Zhao, *Chem. Eur. J.* **2012**, *18*, 2624–2631.
[8] S. K. Klitgaard, K. Egeblad, U. V. Mentzel, A. G. Popov, T. Jensen, E. Taarning, I. S. Nielsen, C. H. Christensen, *Green Chem.* **2008**, *10*, 419–423.
[9] a) H. Zhao, Y. Dong, P. Jiang, G. Wang, J. Zhang, *ACS Appl. Mater. Interfaces* **2015**, *7*, 6451–6461; b) L. Guo, F. Meng, Y. Zeng, Y. Jia, F. Qian, S. Zhang, Q. Zhong, *Mol.Catal.* **2020**, *493*, 111095; c) G. K. Alqurashi, A. Al-Shehri, K. Narasimharao, *RSC Adv.* **2016**, *6*, 71076–71091.
[10] Y. Zhi, K. Li, H. Xia, M. Xue, Y. Mu, X. Liu, *J. Mater. Chem. A* **2017**, *5*, 8697–8704.
[11] Z. Wang, X. Wang, H. Wang, X. Chen, W. Dai, X. Fu, *Appl.Catal. B: Environ.* **2020**, *277*, 119169.
[12] S. Putla, M. H. Amin, B. M. Reddy, A. Nafady, K. A. Al Farhan, S. K. Bhargava, *ACS Appl.Mater. Interfaces* **2015**, *7*, 16525–16535.
[13] D. Wang, J. Huang, F. Liu, X. Xu, X. Fang, J. Liu, Y. Xie, X. Wang, *Catal. Today* **2020**, *339*, 220–232.
[14] S. S. R. Putluru, L. Schill, A. D. Jensen, B. Siret, F. Tabaries, R. Fehrmann, *Appl. Catal. B: Environ.* **2015**, *165*, 628–635.
[15] F. Chen, T. Yang, S. Zhao, T. Jiang, L. Yu, H. Xiong, C. Guo, Y. Rao, Y. Liu, L. Liu, J. Zhou, P. Tu, J. Ni, Q. Zhang, X. Li, *Chin. Chem. Lett.* **2019**, *30*, 2282–2286.
[16] X. Wang, J. Cheng, X. Wang, Y. Shi, F. Chen, X. Jing, F. Wang, Y. Ma, L. Wang, P. Ning, *Chem. Eng. J.* **2018**, *333*, 402–413.
[17] P. Sudarsanam, A. Rangaswamy, B. M. Reddy, *RSC Adv.* **2014**, *4*, 46378–46382.
[18] P. Sudarsanam, H. Li, T. V. Sagar, *ACS Catal.***2020**, *10*, 9555–9584.
[19] B. Hillary, P. Sudarsanam, M. H. Amin, S. K. Bhargava, *Langmuir* **2017**, *33*, 1743–1750.
[20] M. Wang, H. Wu, C. Shen, S. Luo, D. Wang, L. He, C. Xia, G. Zhu, *ChemCatChem* **2019**, *11*, 1935–1942.
[21] V. S. Marakatti, S. Ch. Sarma, B. Joseph, D. Banerjee, S. C. Peter, *ACS Appl. Mater. Interfaces* **2017**, *9*, 3602–3615.
[22] P. Sudarsanam, P. R. Selvakannan, S. K. Soni, S. K. Bhargava, B. M. Reddy, *RSC Adv.* **2014**, *4*, 43460–43469.
[23] N. Nagarjun, M. Jacob, P. Varalakshmi, A. Dhakshinamoorthy, *Mol. Catal.* **2021**, *499*, 111277.

Manuscript received: November 20, 2020
Revised manuscript received: January 10, 2021
Accepted manuscript online: January 21, 2021
Version of record online: February 23, 2021